Fluorescence Quenching in Self-Assembled 2-Aminopurine-Ag^+ Nanofibers

Honors Research Thesis

Presented in partial fulfillment of the requirements for graduation with research distinction in Chemistry in the undergraduate College of Arts and Sciences of The Ohio State University

By Aaron Peter Charnay

The Ohio State University

April 2021

Project Advisor: Dr. Bern Kohler

Department of Chemistry and Biochemistry

Abstract

The binding of Ag+ ion to DNA nucleobases is of interest because of the unique ability of silver ions to direct the formation of novel base pairs. These Ag+-mediated non-canonical base pairing motifs provide the structural elements for DNA-templated silver clusters, which have highly tunable absorption and emission wavelengths from blue to near infrared and thus are strong candidates for the development of novel detection and labeling methods. Atomic force microscopy (AFM) reveals that nanofibers with diameter of tens of nanometers and length of microns are formed when Ag^+ is added to monomeric bases such as adenine and guanosine monophosphate (GMP). However, the molecular-level detail of these self-assembled nanostructures, such as metal binding sites and interaction between bases, that leads to global structure and properties is still unclear. Thiazole orange is a weakly emissive molecule in water but becomes much more fluorescent when intercalated into π stacks. In this project, we used thiazole orange to probe the structure of the supramolecular assemblies formed from mixing Ag^+ and 2-aminopurine, the fluorescent analog of adenine. We show that the π- π stacking between 2-aminopurine molecules is present in the nanofibers, as evident from the enhanced fluorescence of thiazole orange when it is intercalated into the stacks. We further confirmed this result by adding methanol as a denaturant, which significantly reduces the fluorescence from thiazole orange but enhances the fluorescence from 2-aminopurine – both are hallmarks of disrupted π- π stacking. The fluorescent enhancement of thiazole orange in a nucleobase system lacking a covalent backbone is of particular significance as there are to date few examples of such enhancement.

Acknowledgements

I would like to thank Dr. Bern Kohler for his mentorship over the last four years at Ohio State. I would also like to thank Forrest Kohl and Dr. Yuyuan (Tom) Zhang for their support throughout my undergraduate research experience and throughout the writing of this thesis. Thanks also to Dr. Joshua Snyder and Andrew Saks without whom this work would have been impossible. Furthermore, I would like to thank the Kohler Group for all the fun times. I wish you all the best in your future endeavors, academic and otherwise.

Contents

Figure List

1 Introduction

1.1 Biosensors

Biosensors are a class of analytical devices that generate a predictable response for a given biological process or system.[1] An emerging class of biosensor utilizes the unique ability of DNA to bind to its complimentary strand to act as a sensor. DNA is also used as a sensor for a number of metals. Positively-charged metal ions are bound to the negative phosphate backbone of DNA, thereby stabilizing the DNA.[2] In addition, Hg^{2+} and Ag^{+} have high propensities to bind selectively to the nitrogen rich bases.[3] Ag^{+} in particular binds strongly with cytosine bases. Reduction of mismatched C-Ag^{+}-C base pairs in DNA yields red-emissive silver clusters. Further addition of Ag^{+} to the red-emissive complex yields green emission, acting as a selective sensor for Ag^{+}.[4] The fascinating result of DNA-bound metal clusters having tunable emission presents an intriguing direction in the research area of biosensors.

1.2 DNA-Ag^{+} Interactions

Silver clusters of just a few atoms bound to DNA are part of the ever expanding area of research into DNA biosensor technology.[5] These silver clusters (AgCs) can be used in a number of areas ranging from heavy metal identification to cancer imaging.[2, 6] Although these clusters are formed from reducing the Ag^{+}-DNA complexes by $NaBH_4$, X-ray crystallography and mass spectrometry studies show that the clusters themselves are not fully reduced.[7, 8,] It has been proposed that Ag^{+} acts as a glue between the strand and the reduced silver cluster.[9] To date, the binding of Ag^{+} to DNA is not well understood, nor is the formation of extended structures in nucleobase solutions containing Ag^{+}. Such super-structures are present in Ag^{+}-2AP systems that consist of hundreds of nanometers long nanofibers (scheme 1b) and the specific binding motifs of Ag^{+} to 2AP is not known (proposed structure given in scheme 1a).

Current literature suggests that, in DNA strands, Ag^+ selectively binds to the nitrogenous bases instead of the phosphate backbone.[10] The selective binding of Ag^+ to DNA bases is due to the energetic overlap in the silver ion orbitals with the occupied orbitals of ring nitrogens.[11] The ability of clusters to bind selectively to the nitrogen-containing bases results in the sequence-dependent emission of AgCs templated by DNA, which can be tuned from blue to near infrared.[7, 12]

The key insight lacking is in the specific interactions of Ag^+ with the DNA bases, which include adenine (A), cytosine (C), thymine (T), uracil, (U), and guanine (G), and a number of non-canonical nucleobases such as 2-aminopurine (2AP).[12] Monomeric 2AP has a fluorescence quantum yield of 0.68 in aqueous solutions,[13] which is ~1000-fold higher than those of canonical nucleobases, which exhibit very low fluorescence quantum yields due to their ultrashort lifetime of

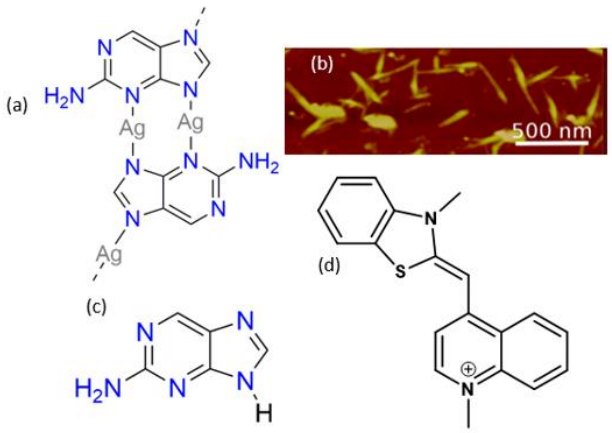

Scheme 1:(a) Possible structure of 2-AP+Ag^+ in a 2:3 ratio. (b) AFM image adapted from reference 23 of 2-AP+ Ag^+ drop cast on a mica disc. (c) 2-aminopurine structure. (d) Thiazole orange structure.

the lowest-lying singlet $\pi\pi^*$ state (< 1 ps).[14] High fluorescence quantum yield is a desirable trait in studying of nucleobase-Ag^+ interactions because of the extremely high sensitivity achievable in fluorescence spectroscopy to any change in emission. This unique property of 2AP coupled with its structural similarity to the canonical nucleobase A makes it an ideal molecule for understanding the interactions of Ag^+ with nucleobases.

1.3 Quenching in 2AP

The fluorescence quantum yield of 2AP is significantly reduced when the bases are π-stacked.[15] In DNA, for example, there is a high degree of π-stacking between adjacent bases and 2AP experiences a significant decrease in fluorescence quantum yield. In the presence of two mole equivalents of Ag^+, the emission of 2AP is quenched by more than 98% (fig 5). It has also been shown via atomic force microscopy (AFM) measurements that 2AP forms extended fibers 100s of nanometers long in the presence of $AgNO_3$ (scheme 1b). This leads to the hypothesis that the subunit shown in Figure 1a is stacked along the long axis of the nanofiber. However, we cannot entirely rule out the possibility that the quenching of 2AP fluorescence is due to metal ion binding.[16, 17]

1.4 Thiazole Orange

Thiazole orange (TO) is a cyanine dye that is mostly non-emissive in aqueous solution due to free rotation about its central bond. However, when the free rotation is inhibited, e.g., when thiazole orange is intercalated between bases in DNA strands, the quantum yield of the dye increases significantly, thus enabling the study of π-π stacking in the nucleobase-Ag^+ systems.[18] Methanol as a cosolvent with water has been shown to effectively denature DNA in aqueous solutions by interrupting base pairing and base stacking. Destacking occurs in the methanol-containing solution as the polarity of the solvent decreases. Solvation of the delocalized π-system for the bases is less favorable (in particular the larger purine bases) in less polar solvent environments.[19]

This research seeks to elucidate whether the cause of fluorescence quenching in 2AP is due to silver binding, or Ag^+-induced π-π stacking. We use TO as a probe for the extent of π- π stacking in different solvent environments. In addition, ion selective electrode measurements were used to analyze Ag^+ binding stoichiometries, providing further information on the interactions of Ag^+ with nucleobases.

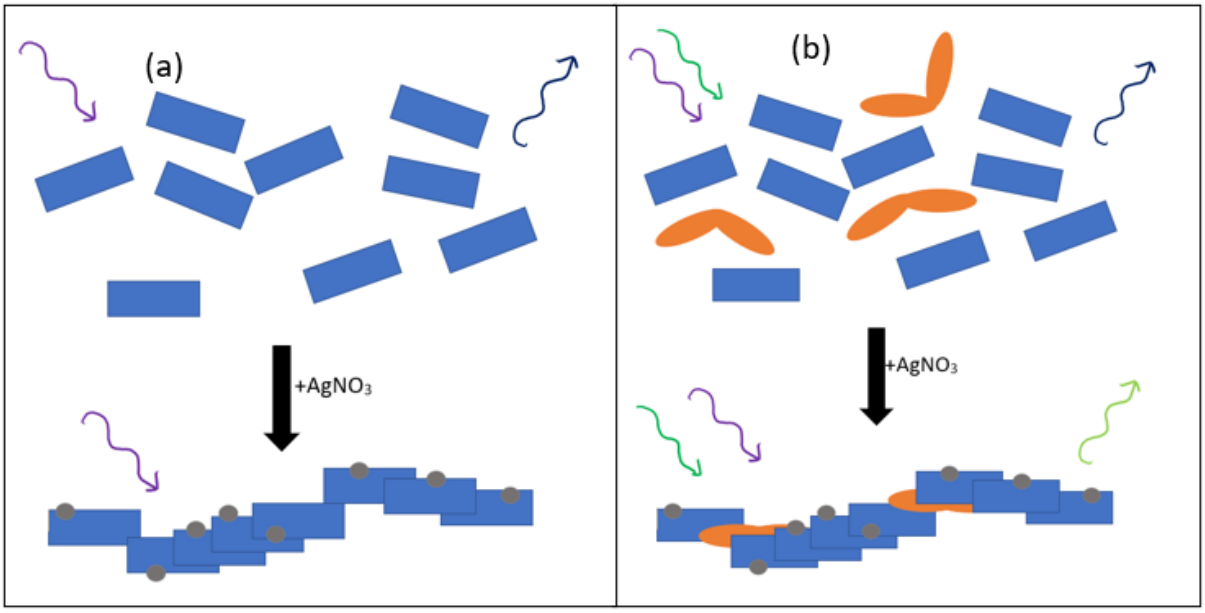

Figure 1: (a) The addition of $AgNO_3$ inducing stacking in 2AP, generating a non-emissive product. Orange pairs of ellipses refer to TO, blue rectangles to 2AP, and grey circles to Ag^+. Before the addition of $AgNO_3$, when 2AP purine is excited (purple wavy arrow) along with TO (green wavy arrow), only the 2AP emits (dark blue wavy arrow). After the addition of $AgNO_3$, when both 2AP and TO are excited, only the TO emits (yellow-green wavy arrow).

2 Theory

2.1 Fluorescence

When a molecule absorbs a photon, it is promoted to a singlet excited state. Typically, the excited-state molecule relaxes from the Franck-Condon region to the minimum of the lowest-energy singlet excited state, where a photon can be emitted (fluorescence). If fluorescence takes place, then the molecule deactivates radiatively. Because the Franck-Condon region always have higher energy than the minimum of the lowest-energy singlet state, the energy of the emitted photon is always lower than that of the absorbed photon (i.e., the wavelength of the emitted photon is always longer than that of the absorbed photon). The energy difference between the absorption and emission maxima is referred to as the Stokes shift (Fig 2).

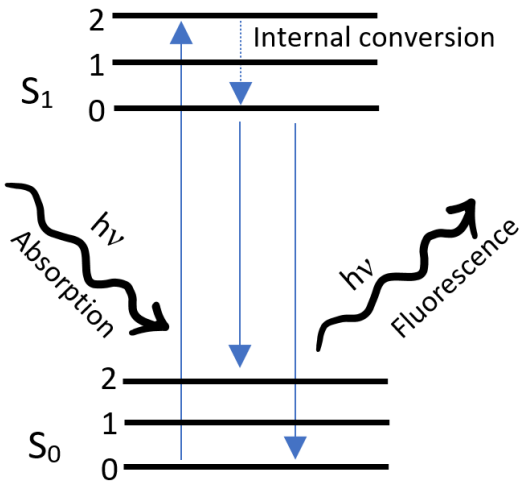

Figure 2: Example of standard Jablonski Diagram depicting a typical fluorescence pathway.

The high fluorescence quantum yield of 2AP arises from its relatively long-lived excited state of 10 ns.[13] This is in stark contrast to the excited state of the canonical nucleobases which decay on the order of hundreds of femtoseconds.[14] 2AP lacks the barrierless transition through the conical intersections that would otherwise allow ultrafast internal conversion from S_1 to S_0.

There are two modes of detection in steady-state fluorescence experiments: emission and excitation. In the emission measurement, the excitation wavelength (λ_{ex}) is kept constant, which is typically set at the absorption maximum of the sample, and the emission spectrum of the sample (fluorescence intensity is plotted against emission wavelengths) is measured by scanning the diffraction grating in the emission monochromator to allow the emission intensities at different wavelengths to be detected by a photomultiplier tube (PMT).

In the excitation measurements, the emission monochromator selects a single wavelength, typically the emission maximum of the sample, and the sample is excited by a range of wavelengths selected by the excitation monochromator. The excitation spectrum is expected to be highly similar to the absorption spectrum.

2.2 Quenching and the Stern-Volmer Equation

The lifetime of an excited state ($\tau_{excited}$) is the inverse of its decay rate, which is the sum of the radiative decay rate (k_r) and the rates of all nonradiative (k_{nr}) decay pathways such as internal conversion and intersystem crossing (eq 1). The fluorescence quantum yield (Q_f) is given by a ratio of the radiative decay rate to the overall rate.[20]

$$\tau_{\text{excited state}} = (k_{\text{total}})^{-1} = (k_r + k_{nr})^{-1}$$
$$Q_F = k_r/(k_r + k_{nr}) \qquad (1)$$

Fluorescence quenching refers to any process that reduces the fluorescence quantum yield. Dynamic quenching takes place when the emitter deactivates upon collision with the quencher, thereby shortening exited-state lifetime of the former. Static quenching takes place when the emitter and the quencher form a ground-state complex, which does not fluoresce after

photoexcitation. A standard quenching process can be modeled with the Stern-Volmer equation (eq 2).[21]

$$I_0 \,/\, I = 1 + k_q \tau_0 [Q] \tag{2}$$

The Stern-Volmer equation suggests a linear relationship between the quencher concentration and the ratio of initial and final emission intensities. Equation 2 shows the Stern-Volmer equation where I_0 is the emission of the fluorophore in the absence of the quencher, I is the emission in the presence of the quencher, k_q is the quenching constant, and τ_o is the excited state lifetime for the emitter. When a ground state complex is formed between the emitter and the quencher, positive deviation from equation 1 is expected. In this case, it is possible to apply the extended S-V equation (eq 3) where there is a quadratic dependence on the concentration of the quencher.[21]

$$I_0 \,/\, I = 1 + \left(K_{sv} + K_g\right)[Q] + K_{sv} K_g [Q]^2 \tag{3}$$

In the system where a ground state complex exists, equation 3 considers that there is a higher degree of quenching. This is also known as static quenching. For the Extended S-V equation, I_0 refers to the emission of the fluorophore in the absence of the quencher, I refers to the emission in the presence of the quencher, where K_{sv} is the linear S-V quenching constant, K_g is the association constant of the ground state and the remaining quantities are identical to Equation 2. In the system where a ground state complex exists, Equation 3 predicts that there is a higher degree of quenching than Equation 2, which is also known as static quenching.

For aqueous 2AP, the absorption and emission bands peak at 305 nm and 370 nm, respectively.[15] When 2AP is incorporated into DNA strands, it can form Watson-Crick base pairing with thymine and a wobble base pair with cytosine.[15] In both cases, stacking with adjacent nucleobases in the same strand is preserved and the radiative lifetime is extended to ~40 ns as predicted by density functional theory (DFT) calculations.[15] This extended lifetime allows nonradiative decay pathways to become competitive therefore reducing the fluorescence quantum yield of 2AP. Metal ions, including Ag^+, binding to fluorophores typically induce fluorescence quenching.[17] A possible mechanism is excited state electron transfer from the fluorophore to the metal ion in which the emissive electronic excited state is not reached because the electron is instead promoted to an unoccupied or partially unoccupied orbital of the metal ion.[22] It is therefore possible that the fluorescence of 2AP is quenched through a ligand-to-metal charge transfer (LMCT), but it is also possible that the fluorescence quenching is due to the π-π stacking of 2AP in the nanofibers, similar to that in DNA single strands and helices.[23]

2.3 Silver Selective Electrode and pH Probe

In this study, two classes of ion selective electrodes were used: a pH probe and a silver selective electrode. The latter is used to quantify the binding of silver ion to ligands. Ion selective electrodes is an electrochemical device that seeks to determine the activity of a certain type of ion that is free, unbound in the solution.[24] These electrodes ultimately give a potential (E) that is logarithmically related to the activity of the ion being measured (eq 4). The factor n relates to the number of electrons transferred for the given oxidation-reduction process. This value is one for the silver selective electrode.[24]

$$E = E^0 - \frac{0.0592}{n} \log C$$

(4)

The Nernst equation (eq 4) shows that for an ideal solution, the voltage measured by the ion selective electrode (ISE) can be plotted against logC and the result should be a line with slope -59.2 mV/ log*C*. When plotting the calibration for the silver selective electrode, the x-axis is labeled as pAg (pAg= -log[Ag^+]). It is therefore expected that potential should decrease with increasing pAg.

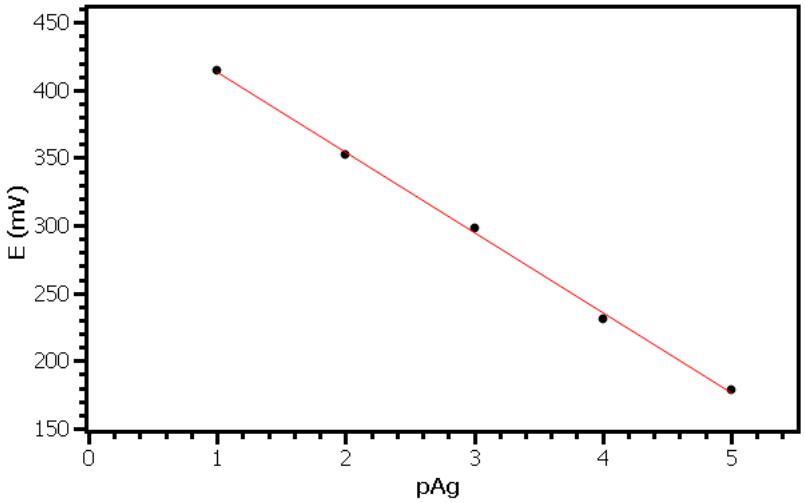

Figure 3: Example calibration curve for silver selective electrode.

$$E = -59.23(pAg) + 472.47$$

(5)

Experimental results for the silver selective electrode agree strongly with Ideal Nernstian behavior with a slope of -59.23 mV/ pAg and an R^2 value of 0.999 (Fig 3).

In the case of the interactions with nucleobases with Ag^+, it is possible to gain information regarding the stoichiometry of binding. If a known concentration of Ag^+ is present in solution with nucleobase, but is undetectable to the electrode, then the Ag^+ is bound.

2.4 UV-Vis

Temperature dependent UV-visible (UV-vis) spectroscopy records a sequence of varying UV-vis spectra at different temperatures. A cuvette containing the analyte is placed in the spectrophotometer, which measures the attenuation or absorption of light at different wavelength in the UV-visible region. Peaks in the absorption spectrum indicate electronic transitions of the absorbing molecule. Changes in the spectrum as a function of temperature indicate a change in the electronic structure of the molecule. In the case of Ag^+-nucleobase assemblies, a change in the absorbance spectrum as a function of temperature may indicate destacking or unbinding of Ag^+.

3 Methods and Materials

2AP (≥99%) and TO (≥90%) were purchased from Sigma Aldrich. $AgNO_3$ (≥99.9%) was purchased from Alfa Aeser. Methanol (99.9%) was purchased from Fisher Chemical. All chemicals were used as received. Stock solutions of 1 and 10 mM 2AP, 75 mM TO, and 100 mM $AgNO_3$ were prepared. Each solution (with a volume of 3 mL) was prepared immediately before measurements. Unless otherwise stated, the final concentrations of 2AP, $AgNO_3$ and TO are 1 mM, 1 mM, and 250 nM, respectively.

$[Ag^+_{free}]$ versus $[Ag^+_{added}]/[2AP]$ (β) measurements were performed using a Mettler Toledo perfectION™ comb Ag/S2 Lemo Combination Electrode. The reported measurement range was 10^{-7} to 1 M and the linear range is 10^{-5} to 1 M. Calibration was done prior to each titration by recording the voltage for standard $AgNO_3$ solutions at 10^{-5}, 10^{-4}, 10^{-3}, 10^{-2}, and 10^{-1} M. Voltage was plotted against pAg (pAg= -log$[Ag^+]$) and the slope and y-intercept obtained from linear fitting was used to determine $[Ag^+_{free}]$ at each value of β. 10 mL solutions of 1 mM 2AP was prepared. Aliquots of 100 mM $AgNO_3$ were added to these solutions in order to maintain

an approximately constant concentration of nucleobase while only varying β. The solutions were under constant stirring and were allowed to equilibrate for two to three minutes before a voltage was measured.

Fluorescence measurements were performed using a Horiba Quantamaster 8000 spectrofluorometer. 2AP fluorescence was measured in a 100 μm cuvette set in a reflection geometry at a 296° angle. This was done instead of using a 1 cm cuvette and a conventional 90° geometry to avoid inner filter effect due to high absorbance at the excitation wavelength. The slit widths for both excitation and emission monochromators were set to 1 nm. This was necessary to prevent saturating the detector due to the high fluorescence quantum yield of 2AP. TO fluorescence measurements were taken using a 1 cm cuvette in a conventional 90° geometry. The concentration of TO in the cuvette 250 nM unless otherwise stated. The slit widths were set to 5 nm for the TO measurements. Integration time of 1 s/nm were used for all measurements.

UV-Vis (including temperature dependent) were performed using a Jasco-815 CD-Spectrometer. All UV-Vis samples were blanked against pure water and averaged over two measurements.

4 Results and Discussion

AFM image of the $AgNO_3$+2AP solution (1 mM 2AP, β = 1) drop cast on a mica substrate reveals nanofibers with lengths of hundreds of nanometers (Scheme 1b). The precise structural motif of these fibers is not known, but it is thought that π-π stacking plays a significant role in the extended structure. Interestingly, there is a significant red shift in the maximum absorption band in 2AP from 305 nm to 330 nm upon addition of $AgNO_3$, which is likely a result of Ag^+ binding and significant structural changes.

As Ag^+ is titrated into solutions containing 2AP, silver ion selective electrode measurements reveal that virtually all Ag^+ (>99%) is bound to 2AP until 1.4 mole equivalents is reached. After this point little additional silver binds (Fig 4b, blue markers). This is similar to the polymeric structure proposed in Scheme 1a where each subunit contains three equivalents of Ag^+ for each two equivalents of 2AP.

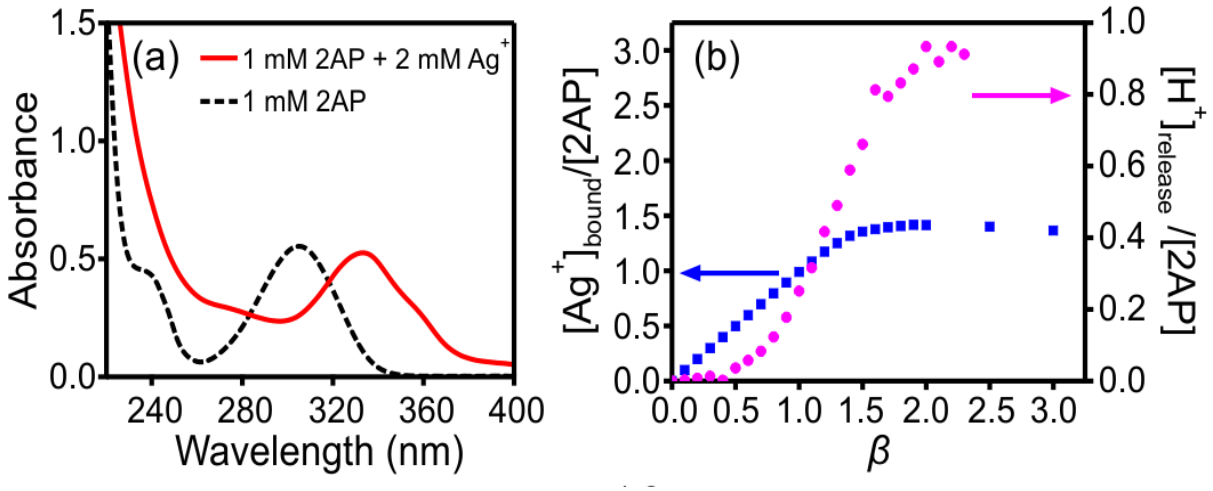

Figure 4: (a) UV-visible spectra of a 2 mM Ag^+/1 mM 2AP aqueous solution (red solid line) and 1 mM 2AP aqueous solution (black dashed line) measured in a 1 mm quartz cell. (b) Bound Ag^+ concentration (blue markers) and released proton concentration (magenta markers) vs. β. Figure reproduced from reference 23 with permission.

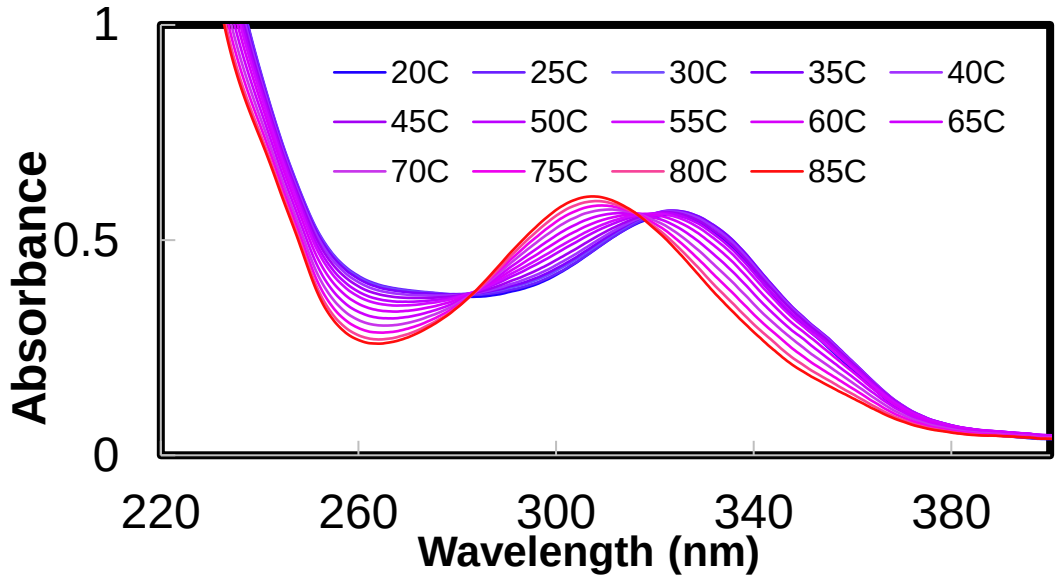

Figure 5: Temperature dependent UV-Vis of 1 mM 2AP at β=2, 1 cm pathlength. Temperature varied between 20-85°C.

For each equivalent of 2AP, one equivalent of hydrogen ions is released into solution (Scheme 1). In fact, pH measurements reveal 0.9 equivalents of hydrogen ions are released for each equivalent of 2AP (Figure 4b, magenta markers).

The temperature dependent UV-vis spectra reveal that as temperature increases, the characteristic peak at 305 nm observed for unbound 2AP is recovered, but a significant red tail remains (Figure 5). One possible explanation is an equilibrium between a silver-bound state and an unbound state. Another explanation is that there are two factors involved in the silver-bound state and one is more strongly affected by temperature. The latter is supported by the persistence of a red tail even at the highest temperatures. The fact that there is a significant red shift in the absorbance spectrum as well as a persistent red tail may be evidence of extensive π- π stacking, but it cannot be definitively determined from the UV-vis spectrum alone.

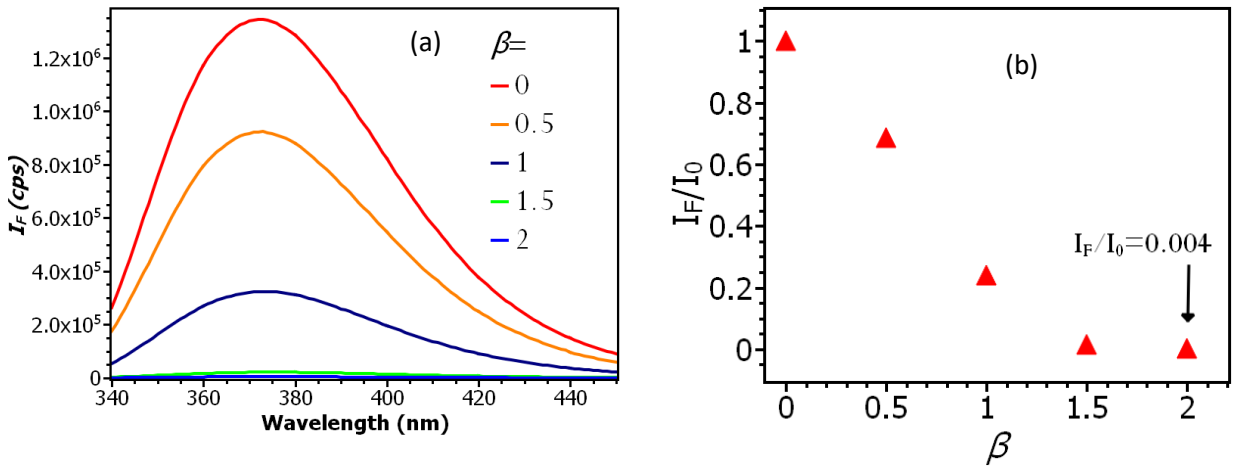

Figure 6:(a) Fluorescence intensity of 2AP at various β. (b) Peak emission intensity at 370 nm as a function of β. For all emission spectra, λex=315 nm.

Fluorescence spectra were recorded for solutions at different β values, the ratio of $[Ag^+]/[2AP]$ (Figure 6a). The emission intensity drops as Ag^+ is added, and importantly, the emission maximum is not shifted as the intensity increases. The emission is nearly fully quenched after 1.5 equivalents of Ag^+ are added (Figure 6b). This agrees with the ion selective electrode

measurement results shown in figure 4b which shows no additional Ag^+ binds after ~1.5 equivalents are added. The change in fluorescence intensity as a function of β does not fit to eq 1 where only dynamic quenching is considered. The Extended Stern-Volmer equation including static quenching (eq 4) also fails to adequately describe the change of I_0/I vs β suggesting Ag^+-bound 2AP is not excited to the emissive state upon absorption, unlike the unbound 2AP molecules (Figure 7).

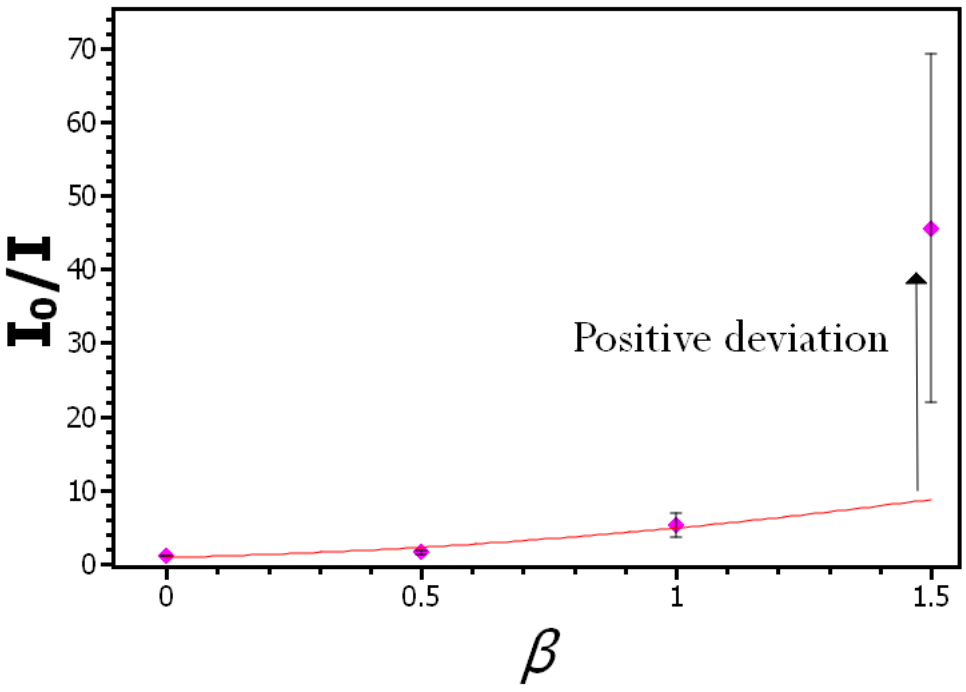

Figure 7: Stern-Volmer plot for emission quenching of 2AP by Ag^+. n=2, error bars = 2σ

The Extended S-V equation still fails to account for a number of key factors. The ground state complex is assumed to be bimolecular, and the quenching mechanism must ultimately consist of a single emissive species interacting with a single quenching species. This fails to

consider additional static quenching that occurs as a result of π-stacking in the Ag^+-2AP assembly. The expected result would then be further positive deviation from the linear S-V quenching.

Clearly the mechanism of quenching is complex and requires a more thorough approach. It is known that at least two distinct interactions are at play; the binding of Ag^+ to 2AP and the stacking interaction between 2AP molecules that contributes to the superstructure apparent in AFM images (scheme 1b).

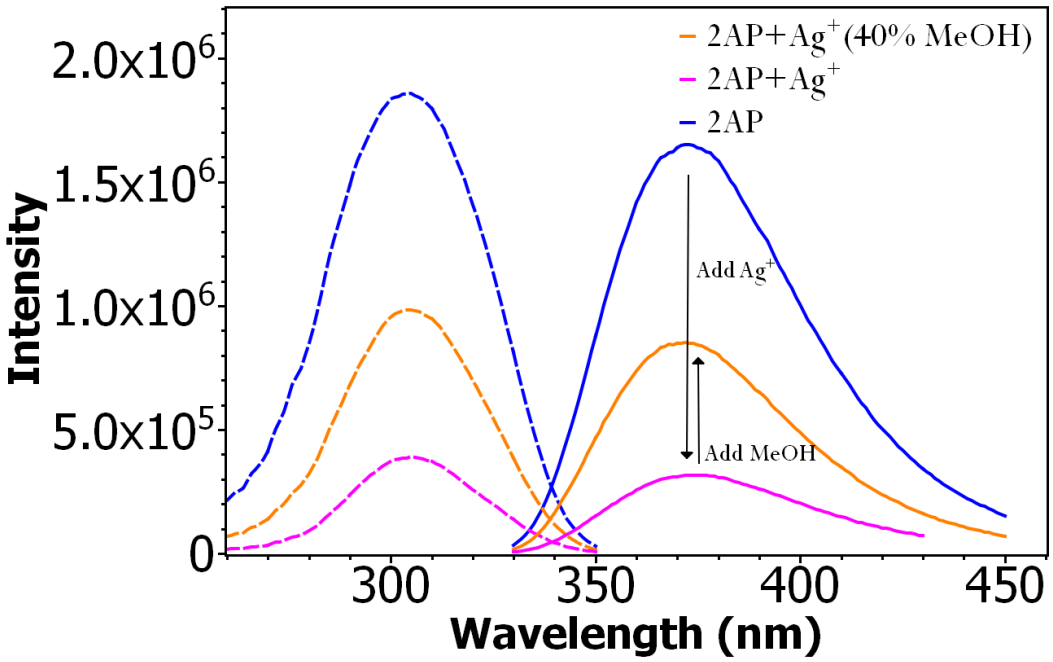

Figure 8: Fluorescence spectra for 2AP. For all emission spectra, λex=315 nm. For all excitation spectra (Dashed curves for coinciding solid curves), λem=370 nm. β = 1 when Ag^+ is present.

The addition of the known denaturant methanol is useful for attempting to isolate the effect binding of Ag^+ and π-π stacking. From figure 8, emission of 2AP was quenched by 80% in the presence of 1 equivalent of Ag^+. When the same solution is prepared in 40% v/v methanol, emission is recovered by 30%, to a value of 50% the original emission. This is too significant an increase to be accounted for by the increase in quantum yield of 2AP in methanol and so denaturation (destacking) has occurred. The fact that the emission is not fully recovered may suggest that binding accounts for the remainder of quenching, or that not all π-π stacking has been eliminated from the structure.

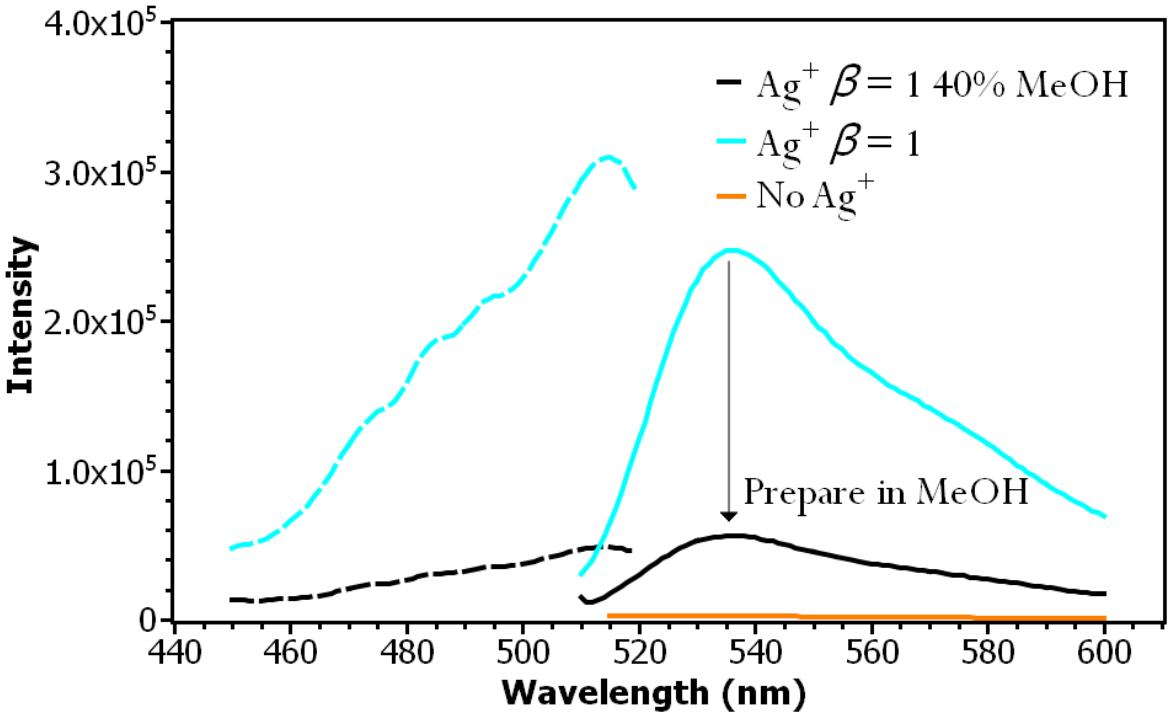

Figure 9: Fluorescence spectra for TO. For all emission spectra, λex=500 nm. For all excitation spectra (Dashed curves for coinciding solid curves), λem=530 nm. All spectra obtained with 1 mM 2AP present.

Thiazole orange is non-emissive in water but has a significant increase in fluorescence when intercalated into π-π stacked structures such as DNA strands.[25, 26, 27] Fig 9 shows that the emission of TO is increased by ~250 fold in the presence of Ag^+ and 2AP. As a control, the emission of TO with Ag^+ was also tested with no 2AP present and little change in the emission was noted. For the solution containing 2AP, Ag^+, and TO, the emission of 2AP is quenched by 80% . When the same solution is prepared in 40% v/v methanol, the 2AP emission is only quenched by 50%, and the TO emission moderately increased by 37 fold. Our result is the definitive evidence that π-π stacking is present in the Ag^+-2AP systems in aqueous solution. The fact that there is residual emission by TO after the addition of methanol suggest that there are still stacks present. It is noteworthy that the vast majority of TO emission is eliminated whereas 2AP remains 50% quenched compared to its original emission. It is therefore useful to attempt to quantify the extent of destacking from the methanol. The simplest explanation would be that there is a linear relationship between the emission of TO and the extent of π-π stacking. In this case it could be asserted that there is 80% less stacking when 40% methanol is present, because the emission intensity of the methanol solution is only 20% compared to that of the aqueous solution.

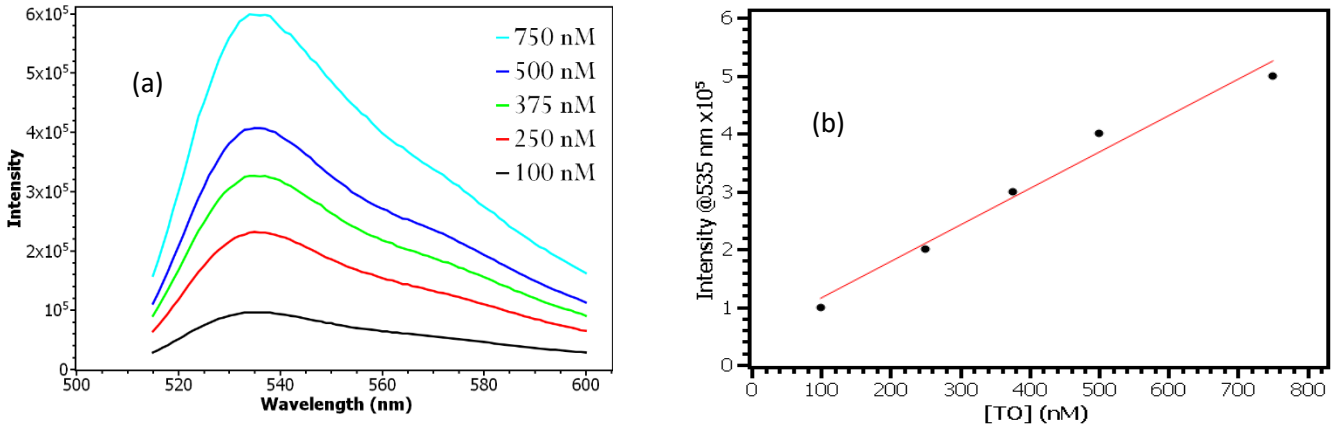

Figure 10: (a) Emission spectra of TO at various concentrations in a 1 cm quartz cell in reflection geometry. (b) Fluorescence intensity at 535 nm for the various concentrations of dye. Excitation Wavelength for all samples = 500 nm.

However, the concentration of TO (nM) is far less than that of the 2AP and Ag^+ (mM). If all TO can intercalate into the 2AP stacks, then the extent of destacking in the methanol solution would be far greater than 80%. This follows because the population of stacked 2AP must be dropped to the nM regime such that only 20% of TO is able to intercalate. To test this hypothesis, we must determine whether all available TO intercalates into 2AP stacks. The concentration of TO was varied from 100 to 750 nM and the emission spectra of the TO + nanofiber solutions were recorded. Figure 10 shows that the emission intensity increases linearly as the concentration increases, suggesting that all TO are intercalated and become emissive. Because the concentration of TO is significantly lower than those of 2AP and Ag^+ and therefore is the limited reagent (250 nM TO and 1 mM 2AP and Ag^+ in Figure 9), we estimate that virtually all 2AP (> 99.9%) is unstacked in the methanol solution to provide just enough intercalation sites for 20% of TO.

Our results suggests that there are two types of structures present in the Ag^+/2AP aqueous solution, and they affect the fluorescence differently. The first type of structure is the nanofiber formed from stacking of the subunits shown in Figure 1, as discussed above. We hypothesize that the second type of structure is small complexes where Ag^+ is bound to 2AP with stoichiometry of less than 1, and without stacking interaction between bases. This follows because the fluorescence of the unbound 2AP is not fully recovered when the nanofiber is completely destacked in the 40% methanol solution, as discussed above (Figure 8). Below we further estimate the fraction of these two populations in the aqueous solution. The fluorescence of the Ag^+/2AP ($\beta = 1$) solution is 20% and 50% of the unbound 2AP in aqueous and 40% methanol solutions, respectively (Figure 8). Because all 2AP are unstacked in the latter, the fluorescence quantum yield of the small complexes is estimated to be 40% of that of the unbound 2AP (taking into account that the quantum

yield of 2AP is 1.2x higher in 40% v/v methanol). Assuming that the quantum yield of the stacked units is ~0, the fraction of 2AP population present in nanofiber and in the small complexes must be approximately 1:1 at β=1.

In proteins there is a kinetic concentration dependence on aggregate formation and an aggregate size concentration dependence.[28, 29] Similarly, the dimerization of TO is based on is known to be concentration dependent.[25] It was therefore of interest to study the effect of concentration of the quenching phenomena observed in 2AP in order to determine if there is a an impact on the extent of stacking indifferent concentration regimes.

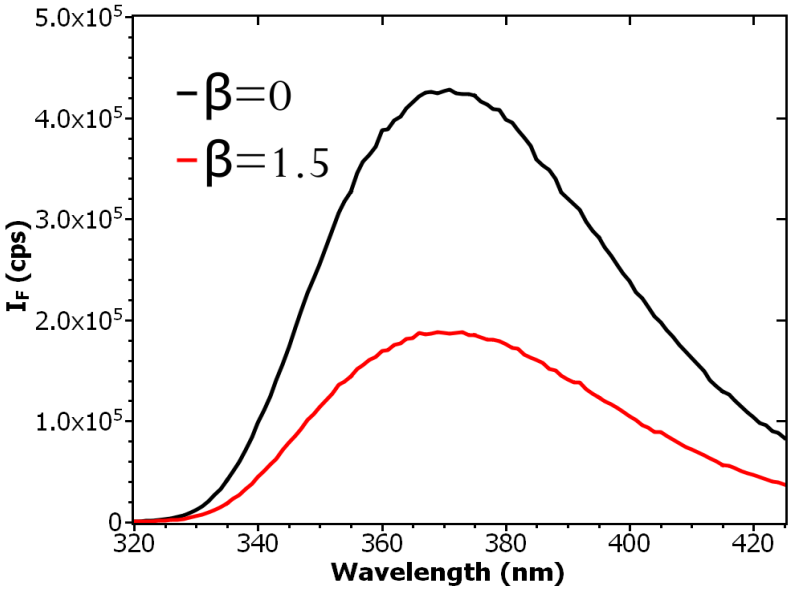

Figure 11: Fluorescence intensity of 2AP at various β. For all emission spectra, λex=315 nm. [2AP] =10 µM

When 1.5 equivalents of Ag^+ are added to 10 µM 2AP, emission is quenched by 55% (Fig 11). This is in contrast to the >98% quenching present in β = 1.5 conditions for the 1 mM 2AP. It has been reported for 1 µM 2AP, at up to β = 100 only 20% of emission is quenched.[13]

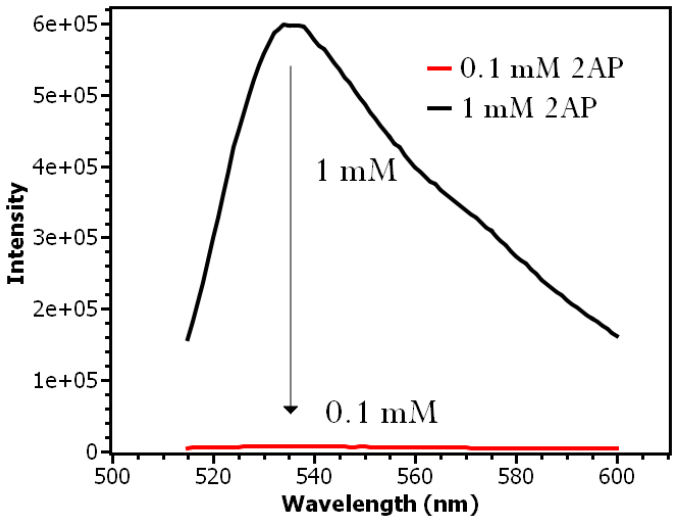

Figure 12: Emission of 750 nM TO in varying concentrations of 2AP and Ag^{+}.

When the concentration of 2AP is varied from 1 mM to 0.1 mM with a constant β and constant concentration of TO, the emission of TO is reduced by ~99% (fig 12). Given that emission of TO is dependent on its ability to intercalate into π- π stacks, this suggests that the structure of the Ag^{+}-2AP system is nearly fully destacked. Like in protein aggregation, the kinetics of aggregation as well as the size of the final aggregates is dependent on the monomer concentration. If aggregate sizes are significantly smaller in the case of the lower concentration system, it would be expected that the number of sites available for TO to intercalate would be impacted. Significantly smaller stacks provide an adequate explanation for the decrease in the observed decrease in quenching when concentration of 2AP is varied.

5 Conclusions and Future Directions

We showed that thiazole orange can be intercalated in the base stacks of the Ag^+-2AP nanofiber, as evident from the 250-fold increase in TO fluorescence intensity. To our knowledge this is the first evidence of TO being used to probe stacking interactions in self-assembled systems lacking a covalent backbone. Our result definitively proves the presence of π-π stacking in Ag^+-2AP. Preparing the nanofiber in 40% v/v methanol/water, where methanol is a known denaturant, significantly decreases the TO emission, and concomitantly increases the 2AP emission, albeit to a lesser extent. This suggests that the self-assembly has been destacked and that quenching is occurring by a different mechanism, namely interaction with bound Ag^+. Further concentration dependent measurements show that the emission of thiazole orange is not as significantly increased when the concentration of 2AP and Ag^+ are decreased. The lack of thiazole orange emission supports the conclusion that within the time frame tested, the extent of π-π stacking in lower concentration solutions is lower and the remaining quenching comes from Ag^+. Future directions for this work include examining the extent to which the lesser stacking in the lower concentration regime is a kinetic phenomenon. Annealing these samples consistently results in cloudy solutions that are not suitable for fluorescence measurements, and so time dependent measurements could be taken to monitor the kinetics of π-π stack formation via the emission of TO.

6 References

(1) DNA Biosensors and Microarrays | Chemical Reviews https://pubs-acs-org.proxy.lib.ohio-state.edu/doi/10.1021/cr0684467 (accessed Apr 3, 2021).

(2) Zhou, W.; Saran, R.; Liu, J. Metal Sensing by DNA. *Chem. Rev.* **2017**, *117* (12), 8272–8325. https://doi.org/10.1021/acs.chemrev.7b00063.

(3) Izatt, R. M.; Christensen, J. J.; Rytting, J. H. Sites and Thermodynamic Quantities Associated with Proton and Metal Ion Interaction with Ribonucleic Acid, Deoxyribonucleic Acid, and Their Constituent Bases, Nucleosides, and and Nucleotides. *Chem. Rev.* **1971**, *71* (5), 439–481. https://doi.org/10.1021/cr60273a002.

(4) Ono, A.; Cao, S.; Togashi, H.; Tashiro, M.; Fujimoto, T.; Machinami, T.; Oda, S.; Miyake, Y.; Okamoto, I.; Tanaka, Y. Specific Interactions between Silver(I) Ions and Cytosine–Cytosine Pairs in DNA Duplexes. *Chem. Commun.* **2008**, No. 39, 4825–4827. https://doi.org/10.1039/B808686A.

(5) Mehrotra, P. Biosensors and Their Applications – A Review. *J. Oral Biol. Craniofacial Res.* **2016**, *6* (2), 153–159. https://doi.org/10.1016/j.jobcr.2015.12.002.

(6) Zhang, Q.; Yang, M.; Zhu, Y.; Mao, C. Metallic Nanoclusters for Cancer Imaging and Therapy. *Curr. Med. Chem.* **2018**, *25* (12), 1379–1396. https://doi.org/10.2174/0929867324666170331122757.

(7) Petty, J. T.; Sergev, O. O.; Kantor, A. G.; Rankine, I. J.; Ganguly, M.; David, F. D.; Wheeler, S. K.; Wheeler, J. F. Ten-Atom Silver Cluster Signaling and Tempering DNA Hybridization. *Anal. Chem.* **2015**, *87* (10), 5302–5309. https://doi.org/10.1021/acs.analchem.5b01265.

(8) Terrón, A.; Tomàs, L.; Bauzá, A.; García-Raso, A.; Fiol, J. J.; Molins, E.; Frontera, A. The First X-Ray Structure of a Silver–Nucleotide Complex: Interaction of Ion Ag(I) with Cytidine-5′-Monophosphate. *CrystEngComm* **2017**, *19* (39), 5830–5834. https://doi.org/10.1039/C7CE01400G.

(9) He, C.; Goodwin, P. M.; Yunus, A. I.; Dickson, R. M.; Petty, J. T. A Split DNA Scaffold for a Green Fluorescent Silver Cluster. *J. Phys. Chem. C* **2019**, *123* (28), 17588–17597. https://doi.org/10.1021/acs.jpcc.9b03773.

(10) Berti, L.; Burley, G. A. Nucleic Acid and Nucleotide-Mediated Synthesis of Inorganic Nanoparticles. *Nat. Nanotechnol.* **2008**, *3* (2), 81–87. https://doi.org/10.1038/nnano.2007.460.

(11) Soto-Verdugo, V.; Metiu, H.; Gwinn, E. The Properties of Small Ag Clusters Bound to DNA Bases. *J. Chem. Phys.* **2010**, *132* (19), 195102. https://doi.org/10.1063/1.3419930.

(12) Petty, J. T.; Zheng, J.; Hud, N. V.; Dickson, R. M. DNA-Templated Ag Nanocluster Formation. *J. Am. Chem. Soc.* **2004**, *126* (16), 5207–5212. https://doi.org/10.1021/ja031931o.

(13) Saran, R.; Yao, L.; Hoang, P.; Liu, J. Folding of the Silver Aptamer in a DNAzyme Probed by 2-Aminopurine Fluorescence. *Biochimie* **2018**, *145*, 145–150. https://doi.org/10.1016/j.biochi.2017.07.001.

(14) Chris T. Middleton; Kimberly de La Harpe; Charlene Su; Yu Kay Law; Carlos E. Crespo-Hernández; Bern Kohler. DNA Excited-State Dynamics: From Single Bases to the Double Helix. *Annu. Rev. Phys. Chem.* **2009**, *60*, 217–239. https://doi.org/59.032607.093719.

(15) Jean, J. M.; Hall, K. B. 2-Aminopurine Fluorescence Quenching and Lifetimes: Role of Base Stacking. *Proc. Natl. Acad. Sci. U. S. A.* **2001**, *98* (1), 37–41.

(16) Fabbrizzi, L.; Licchelli, M.; Pallavicini, P.; Sacchi, D.; Taglietti, A. Sensing of Transition Metals through Fluorescence Quenching or Enhancement. A Review. *Analyst* **1996**, *121* (12), 1763–1768. https://doi.org/10.1039/AN9962101763.
(17) Masuhara, H.; Shioyama, H.; Saito, T.; Hamada, K.; Yasoshima, S.; Mataga, N. Fluorescence quenching mechanism of aromatic hydrocarbons by closed-shell heavy metal ions in aqueous and organic solutions https://pubs.acs.org/doi/pdf/10.1021/j150668a026 (accessed Apr 6, 2021). https://doi.org/10.1021/j150668a026.
(18) Nygren, J.; Svanvik, N.; Kubista, M. The Interactions between the Fluorescent Dye Thiazole Orange and DNA. *Biopolymers* **1998**, *46* (1), 39–51. https://doi.org/10.1002/(SICI)1097-0282(199807)46:1<39::AID-BIP4>3.0.CO;2-Z.
(19) Chen, J.; Kohler, B. Base Stacking in Adenosine Dimers Revealed by Femtosecond Transient Absorption Spectroscopy. *J. Am. Chem. Soc.* **2014**, *136* (17), 6362–6372. https://doi.org/10.1021/ja501342b.
(20) Introduction to Fluorescence. In *Principles of Fluorescence Spectroscopy*; Lakowicz, J. R., Ed.; Springer US: Boston, MA, 2006; pp 1–26. https://doi.org/10.1007/978-0-387-46312-4_1.
(21) Gehlen, M. H. The Centenary of the Stern-Volmer Equation of Fluorescence Quenching: From the Single Line Plot to the SV Quenching Map. *J. Photochem. Photobiol. C Photochem. Rev.* **2020**, *42*, 100338. https://doi.org/10.1016/j.jphotochemrev.2019.100338.
(22) Sutin, N.; Creutz, C. Electron-Transfer Reactions of Excited States. *J. Chem. Educ.* **1983**, *60* (10), 809. https://doi.org/10.1021/ed060p809.
(23) Snyder, J. A.; Charnay, A. P.; Kohl, F. R.; Zhang, Y.; Kohler, B. DNA-like Photophysics in Self-Assembled Silver(I)–Nucleobase Nanofibers. *J. Phys. Chem. B* **2019**, *123* (28), 5985–5994. https://doi.org/10.1021/acs.jpcb.9b00660.
(24) Koryta, J. Ion-Selective Electrodes. *Annu. Rev. Mater. Sci.* **1986**, *16* (1), 13–27. https://doi.org/10.1146/annurev.ms.16.080186.000305.
(25) Biancardi, A.; Biver, T.; Marini, A.; Mennucci, B.; Secco, F. Thiazole Orange (TO) as a Light-Switch Probe: A Combined Quantum-Mechanical and Spectroscopic Study. *Phys. Chem. Chem. Phys.* **2011**, *13* (27), 12595–12602. https://doi.org/10.1039/C1CP20812H.
(26) Kang, B. H.; Gao, Z. F.; Li, N.; Shi, Y.; Li, N. B.; Luo, H. Q. Thiazole Orange as a Fluorescent Probe: Label-Free and Selective Detection of Silver Ions Based on the Structural Change of i-Motif DNA at Neutral PH. *Talanta* **2016**, *156–157*, 141–146. https://doi.org/10.1016/j.talanta.2016.05.006.
(27) Large Dynamic Stokes Shift of DNA Intercalation Dye Thiazole Orange has Contribution from a High-Frequency Mode | Journal of the American Chemical Society https://pubs-acs-org.proxy.lib.ohio-state.edu/doi/10.1021/ja056862n (accessed Apr 1, 2021).
(28) Kodaka, M. Interpretation of Concentration-Dependence in Aggregation Kinetics. *Biophys. Chem.* **2004**, *109* (2), 325–332. https://doi.org/10.1016/j.bpc.2003.12.003.
(29) Frenkel, Y. V.; Clark, A. D.; Das, K.; Wang, Y.-H.; Lewi, P. J.; Janssen, P. A. J.; Arnold, E. Concentration and PH Dependent Aggregation of Hydrophobic Drug Molecules and Relevance to Oral Bioavailability. *J. Med. Chem.* **2005**, *48* (6), 1974–1983. https://doi.org/10.1021/jm049439i.